Contents lists available at ScienceDirect

Transactions of Nonferrous Metals Society of China

36(2026) 638−648

www.tnmsc.cn

Preparation of high-purity tellurium based on simulation-assisted zone refining

Qing-hua TIAN [a], Zhi-qiang HE [a], Zhi-peng XU [a,*], Hai-bei WANG [b], Liu ZHU [c]

[a] School of Metallurgy and Environment, Central South University, Changsha 410083, China;

[b] BGRIMM Technology Group Co., Ltd., Beijing 100160, China;

[c] Guangdong First Rare Materials Co., Ltd., Qingyuan 511517, China

Abstract: The effect of temperature on molten zone length was investigated through simulation to optimize the control of molten zone length during the experimental process. The temperature gradient distribution within the molten zone during zone refining was simulated using COMSOL Multiphysics software and experimentally validated. The simulated molten zone length showed good agreement with the actual measured length. The experimental study of tellurium purification by zone refining was conducted under the following conditions: three passes of zone refining, a hydrogen flow rate of 0.5 L/min, and molten zone movement speeds of 0.5 and 1.0 mm/min. The results demonstrated that the removal efficiencies of impurities such as Ca and Cu exceeded 95%, while the removal efficiency of phosphorus (P) reached over 70%. And the purity of tellurium reached 6N.

Key words: high purity tellurium; simulation; zone refining; molten zone length

1 Introduction

High-purity materials are essential for fundamental research and practical applications like semiconductor devices, infrared-detecting core components, and 5G communications. For example, Te with a purity of 5N is a crucial part of Bi_2Te_3-type alloys used to make power generators or thermoelectric coolers [1] and serves as a primary raw material for CdTe solar cells [2,3]. For tellurium in Cu_2Te [4], HgTe, and HgCdTe [5] compounds, a purity of 6N−7N is required. These compounds are primarily used in devices such as spectral analyzers, infrared modulators, and nuclear radiation detectors. Although high-purity tellurium can be produced by a number of methods, zone refining is the most efficient method [6−8].

There are stringent requirements for the accurate regulation of temperature in the zone refining process [9−12]. The accurate control of the temperature zone in the zone refining process, and thus the control of the length of the molten zone, is currently a research hotspot. It has been well studied by researchers through simulation [13−15]. For example, LI et al [16] investigated the silicon purification process and demonstrated that the temperature distribution within the melt is influenced by both the number of induction heating sources and the position of the melt pool. By optimizing the numerical model through the input parameters, the temperature distribution and gradient in the silicon melt can meet the requirement of silicon vacuum induction refining. In the case of lanthanum purification, CHEN et al [17] employed the zone refining technique, establishing a simulation

Corresponding author: *Zhi-peng XU, Tel: +86-18175150670, E-mail: zhipeng.xu@csu.edu.cn

https://doi.org/10.1016/S1003-6326(25)66987-1

Received 2 May 2024; accepted 17 January 2025

model using finite element analysis. And the results showed good agreement between the simulation and the experimental findings. ROUSSOPOULOS and RUBINI [18] explored the thermal field distribution of indium antimonide during the zone refining process and derived the correlation between the length of the molten zone and key parameters through process modeling.

At present, zone refining of tellurium is still poorly investigated, and a major challenge is the difficulty in effectively controlling the molten zone length during the refining process. Experimentally investigating the zone refining temperature and molten zone length is time-consuming and energy-intensive. These issues can be effectively addressed through numerical simulation combined with experimental verification [19−21]. To assist in selecting the temperature parameters, in this study, the molten zone length in the zone refining process was first simulated, and then validation experiments were conducted. Subsequently, tellurium purification tests using zone refining were performed based on the simulation results, and the purity and impurity distribution of the tellurium were examined.

2 Simulation

2.1 Geometrical modelling

The resistance heating method was employed in the experiment, with the key components of the system being the heater, graphite boat, and metal tellurium. A geometric model was established using COMSOL Multiphysics software, and its sketch is shown in Fig. 1. The main parameters of the geometric model are listed in Table 1.

The heater has a 70 mm-wide insulation layer, a 60 mm-wide heat source, and a 5 mm outer extension of insulation on each side of the heat source. The zone refining system was placed in the air domain to simulate the heat dissipation process.

2.2 Governing equations

Zone refining of tellurium involves not only heat transfer but also liquid flow and solute diffusion. Numerical simulations provide valuable data that are difficult to obtain from experiments, thereby reducing experimental costs and shortening the experimental timeline. Therefore, it is important to perform numerical simulations of the tellurium zone refining process. Temperature significantly affects the physical properties of materials, and the accurate input of material parameters during simulation is crucial to reflecting the actual system conditions [13]. In this study, COMSOL Multiphysics finite element software was used for the simulation, with the physical parameters of the materials listed in Table 2.

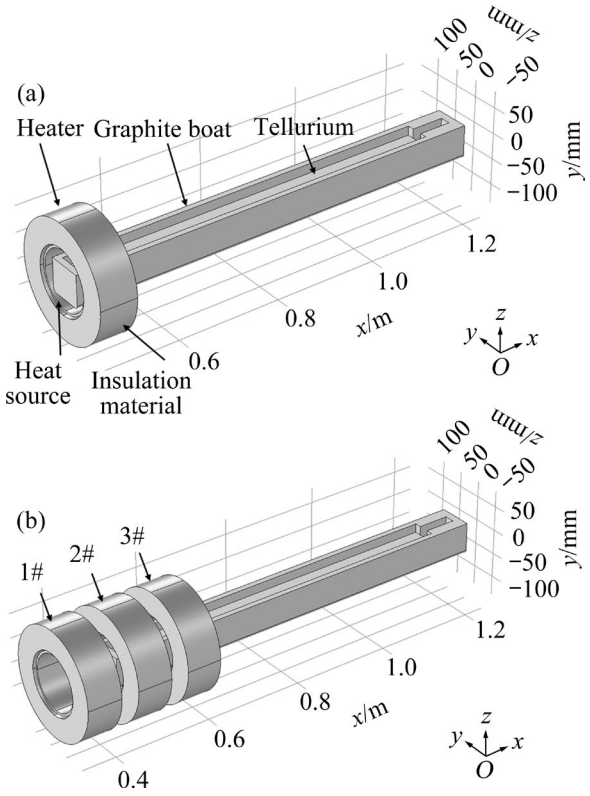

Fig. 1 Geometrical model of zone refining reactor: (a) Single heater; (b) Multiple heaters

Table 1 Geometric model parameters

Region	Parameter	Value
Graphite boat	Length/mm	800
	Width/mm	74
	High/mm	64
	Thickness of side/mm	12
	Thickness of bottom/mm	16
Tellurium	Length/mm	710
	Width/mm	50
	High/mm	40
Heater	Width of insulation/mm	70
	Thickness of insulation/mm	60
	Width of heat source/mm	60
	Spacing of heater/mm	105

Table 2 Performance parameters of materials during simulation

Region	Parameter	Value
Graphite boat	Density/(kg·m^{-3})	1710
	Thermal conductivity/(W·m^{-1}·K^{-1})	100
	Specific heat capacity/(J·kg^{-1}·K^{-1})	1800
	Emissivity	0.8
Insulation	Density/(kg·m^{-3})	230
	Specific heat capacity/(J·kg^{-1}·K^{-1})	210
	Thermal conductivity/(W·m^{-1}·K^{-1})	0.153
	Emissivity	0.2
Heat source	Density/(kg·m^{-3})	1225
	Specific heat capacity/(J·kg^{-1}·K^{-1})	1006.4
	Thermal conductivity/(W·m^{-1}·K^{-1})	0.9
Tellurium	Emissivity	0.3

Mathematical models were developed by analyzing conduction heat transfer in solid components [15,22,23]. The effective conduction coefficient was used to approximate the convective heat transfer as follows:

$$\rho C_p \frac{\partial T}{\partial t} + \rho C_p v \cdot \nabla T = \nabla \cdot (\lambda \nabla T) + Q \quad (1)$$

where ρ, C_p and T represent density (g/cm³), specific heat capacity (J/(kg·°C)), and temperature, respectively. The parameter λ represents thermal conductivity, Q is the internal heat source generated by radiation interactions within the system, and v is the velocity. The initial condition defines the temperature distribution in the zone at time zero (t=0), while the boundary condition describes the temperature or heat flux at the zone boundary. In the tellurium zone refining process, convective and radiative heat transfer are primarily combined. In the absence of forced convection, convective heat transfer is negligible. Therefore, the boundary conditions can be expressed as follows:

$$(1-\varepsilon)G = J - \varepsilon\sigma T^4 \quad (2)$$

where ε denotes emissivity, G and J represent the incident radiation and effective radiation, respectively, and σ is the blackbody radiation constant. Additionally, the following assumptions were made: (1) The material properties are uniform and isotropic; (2) The density and viscosity of the tellurium material are constant, and the tellurium melt behaves as an incompressible Newtonian fluid; (3) The surface of the tellurium melt is flat.

2.3 Grid meshing

Considering the reactor's characteristics and the limitations of the grid node structure, a free tetrahedral mesh was used for computational grid generation, as shown in Fig. 2.

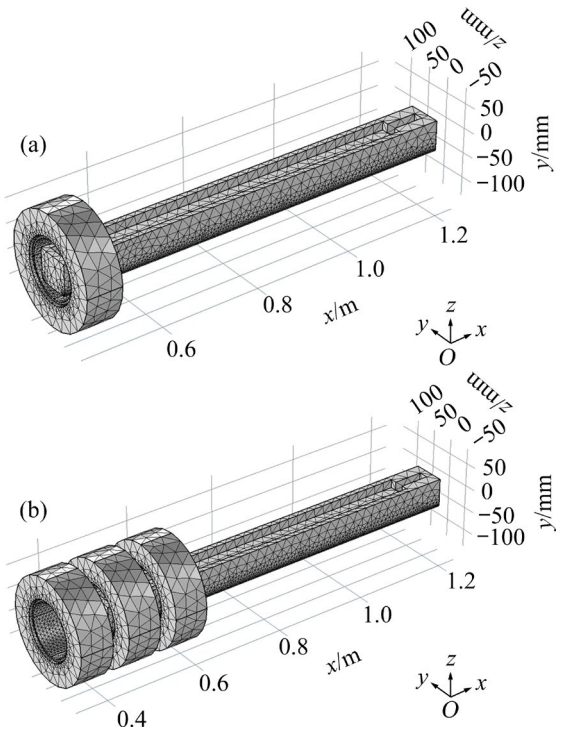

Fig. 2 Zone refining reactor meshing: (a) Single heater; (b) Multiple heaters

After meshing, the total number of elements was 916162, with a minimum orthogonal quality of 0.05. The average cell quality was 0.66, indicating that the free tetrahedral mesh had acceptable quality.

3 Experimental

To verify the accuracy of the simulation, zone refining experiments of tellurium were conducted. As illustrated in Fig. 3, the zone refining equipment consists primarily of furnace body, control cabinet, crucible, and movable trolley. To prevent oxidation, the experiments were conducted under a reducing hydrogen atmosphere, which also helped remove selenium impurities [24,25]. The control cabinet regulated the temperature of each heater, the movement rate of the trolley (molten zone speed), and the gas flow rate. The heaters were numbered as 1#, 2#, and 3#, with Heater #2 being the main heater and Heaters #1 and #3 serving as auxiliary

heaters. Figure 3(b) shows the graphite boat after loading the raw material. The equipment was manufactured by Gaomi Putte Electronic Equipment Co., Ltd., model number PTZR-103, with dimensions of 1750 mm × 600 mm × 1250 mm (length, width, and height). The 5N-grade gases used in the experiment were supplied by Nanchang Xiangfeng Experimental Equipment Co,.

The raw material used for the experiments was 5N tellurium ingot, with approximately 5.0 kg of raw material used in each experiment. The impurity contents in the raw material are listed in Table 3. The main impurities were Se, Cu, Si, S, and Bi. Therefore, special attention must be paid to these impurities during the experiment. Impurities such as Cr, Mn, Fe, and Ni had low concentrations and were considered negligible. The experimental conditions are listed in Table 4.

The sampling method is shown in Fig. 4. The tellurium rods were 70 cm in total length and were divided equally into seven segments, with the sampling points located at x=10 cm, x=20 cm, x=30 cm, x=40 cm, x=50 cm, and x=60 cm. The samples were tested using Glow Discharge Mass Spectrometry (GDMS).

4 Results and discussion

4.1 Effect of temperature on molten zone length

Temperature was the main factor affecting the distribution characteristics of the molten zone. Under the conditions of a heater width of 60.0 mm and an ambient temperature of 25 °C, the temperature distribution of the tellurium rod was simulated when the temperatures of Heater #2 were set as 600, 650, 700, and 750 °C, respectively. The simulation results are shown in Fig. 5. When the temperatures of Heater #2 were 600 and 650 °C, the highest temperatures in the molten zone were 378 and 426 °C, respectively, which did not reach the melting point of tellurium. This indicates that tellurium would not melt during the experiment. When the temperatures of Heater #2 were 700 and 750 °C, the highest temperatures in the center of the

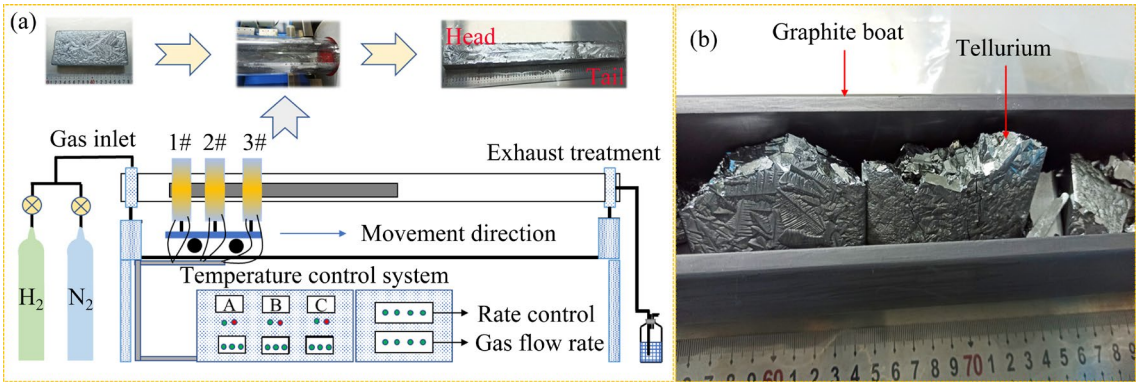

Fig. 3 Diagram of experimental setup (a) and photograph of graphite boat and raw material (b)

Table 3 Contents of experimental materials (μg/kg)

Experiment No.	Li	Na	Mg	Si	P	S	Ca	Ti	Cr
1	3.2	7.2	6.2	10.1	5.6	8.6	11.0	<0.5	<1.0
2	<0.5	<0.5	<0.5	11.1	8.6	7.3	<5.0	<0.5	<1.0
Experiment No.	Mn	Fe	Ni	Cu	Zn	Se	Ag	Bi	Total
1	<0.5	<1.0	<0.5	190.0	1.6	1100.0	8.4	12.0	1363.9
2	<0.5	<1.0	<0.5	76.0	<1.0	846.0	<5.0	5.7	954.7

Table 4 Experimental parameters of zone refining

Experiment No.	Zone length/cm	Moving rate/(mm·min^{-1})	Zone refining pass	H_2 flow rate/(L·min^{-1})
1	6−7	0.5	3	0.5
2	6−7	1.0	3	0.5

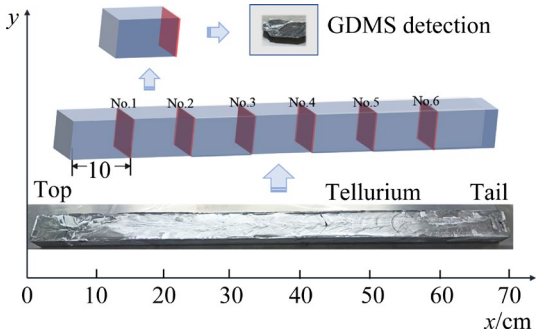

Fig. 4 Schematic diagram of sampling locations

molten zone reached 467.3 and 514.6 °C, and the lengths of the zone where the temperature reached the melting point of tellurium were 40.0 and 61.4 mm, respectively. The head of the tellurium rods was relatively easy to melt during the experiment. However, when the temperature of Heater #2 reached 750 °C, a stable molten zone still could not form, indicating that heating the tellurium with a single heater was insufficient to meet the experimental requirements in this system.

4.2 Effect of heater width on molten zone length

The width of the heater (the width of the heat source) directly affects the length of molten zone. The use of narrow heaters facilitates control over the length of molten zone but is susceptible to environmental influences, which can lead to instability in molten zone. In contrast, wider heaters have better insulation performance, which helps maintain the stability of the temperature gradient during the zone refining process. For low melting point metals, narrow heaters are generally used (e.g., indium [26]). While wider heaters are preferred for the purification of metals with higher melting points, and induction heating or electron beam heating is commonly employed for those metals [27,28]. Under the condition that the temperature of Heater #2 is 700 °C and the ambient temperature is 25 °C, computational models were designed with heater widths of 40.0, 60.0, 80.0, and 100.0 mm, and the simulation results are shown in Fig. 6.

As shown in Fig. 6(a), when the width of the heater was 40.0 mm, the maximum temperature in the tellurium rod reached 394.0 °C. When the width of the molten zone was increased to 60.0, 80.0, and 100.0 mm, the maximum temperatures of the tellurium rod in the temperature field reached 467.3, 519.9, and 556.1 °C, respectively. The lengths of the temperature gradient needed to reach the tellurium melting point of 452 °C were 40.0, 76.6, and 104.4 mm, respectively. The results indicated that when the length of the heater was 80.0 mm, the experimental requirement of controlling the molten zone to about 70.0 mm could be achieved. However, a phenomenon of significant irregularity in the molten zone occurred during the experiments, which led to the migration of impurities to the edges of the tellurium rod, thereby reducing the efficiency of impurity removal. Therefore, the use of wider heaters was not favorable for controlling the length of the molten zone during the tellurium

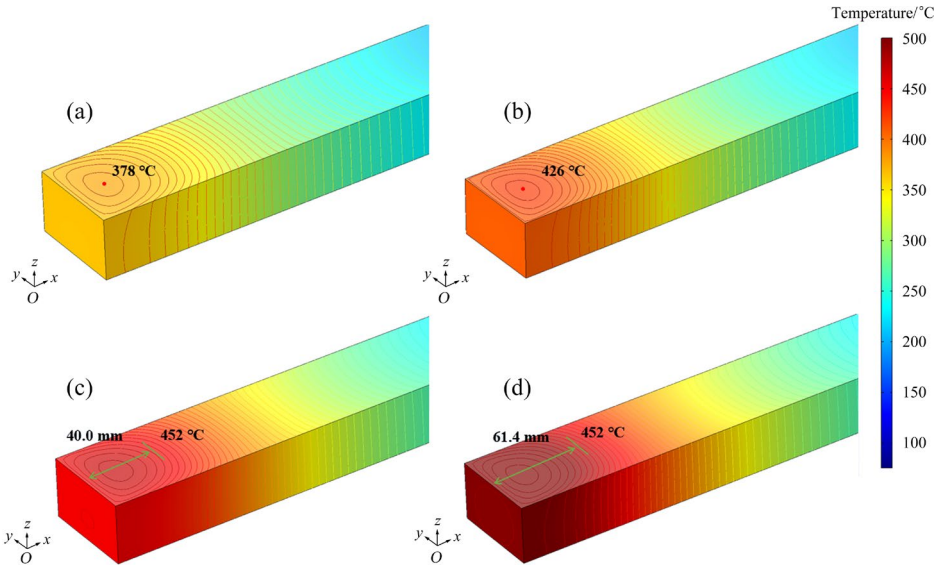

Fig. 5 Temperature distribution of tellurium ingots at different zone refining temperatures: (a) 600 °C; (b) 650 °C; (c) 700 °C; (d) 750 °C

zone refining process. Thus, a heater width of 60.0 mm was deemed reasonable for the purification of tellurium.

4.3 Effect of multiple heaters on molten zone length

From the above analysis, it can be seen that a single heater could not form a stable and regular molten zone. The use of multi-heater synergistic temperature control can achieve better results. Figure 7 shows the temperature distribution in the melt zone, where Heater #2 was set as 700 °C in both experiments. In Experiment 1, Heaters #1 and #3 were set as 630 °C, while in Experiment 2, Heaters #1 and #3 were set as 610 °C. The simulation results indicated that multi-heater synergistic temperature control resulted in a dense distribution of the temperature gradient in the molten zone, which was conducive to controlling the length of the molten zone during the experimental process [29].

Figure 7(a) showed that with the main heater and auxiliary heater temperatures set at 700 and 630 °C, respectively, both the simulated and actual

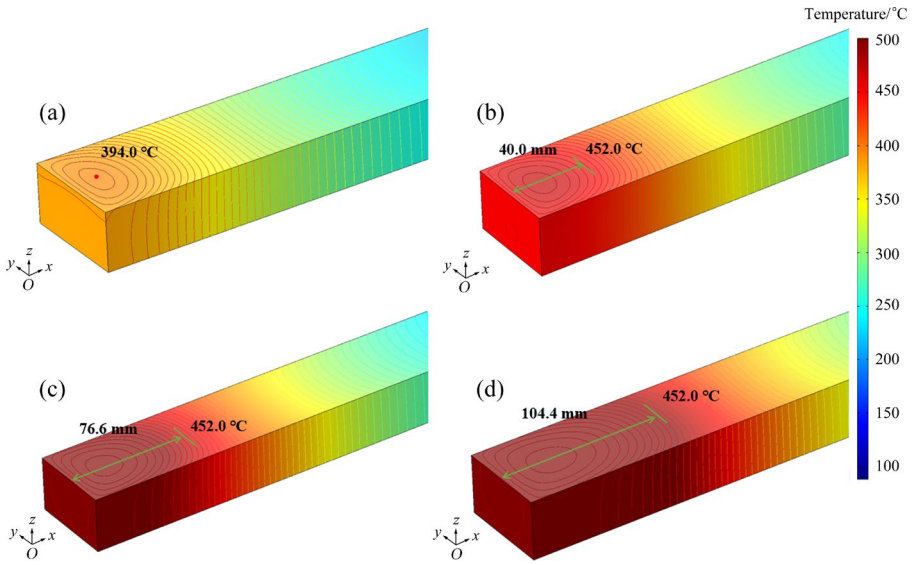

Fig. 6 Temperature distribution of tellurium ingots with different heater widths: (a) 40.0 mm; (b) 60.0 mm; (c) 80.0 mm; (d) 100.0 mm

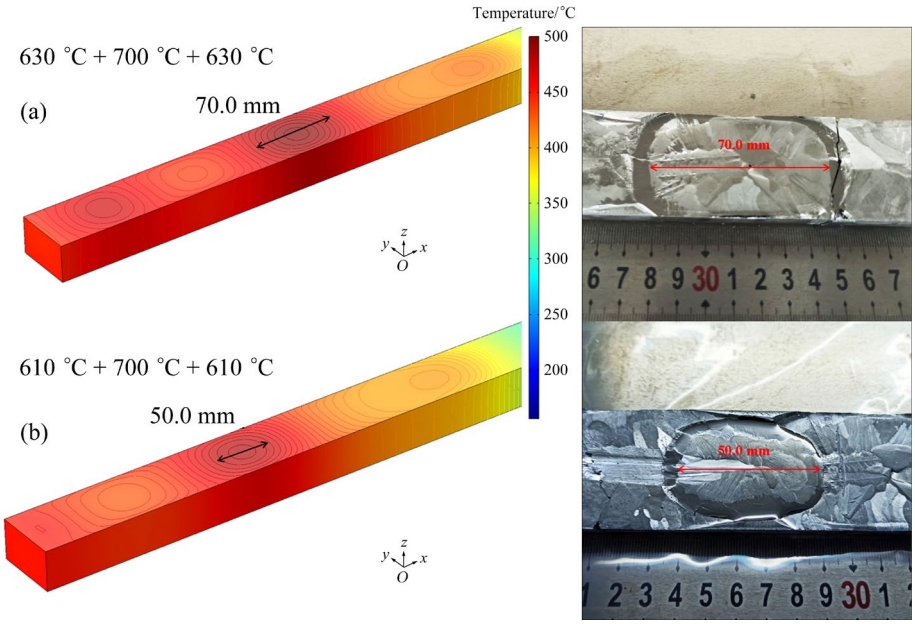

Fig. 7 Simulated melt length vs experimental melt length: (a) 1#+2#+3# (630 °C + 700 °C + 630 °C); (b) 1#+2#+3# (610 °C + 700 °C + 610 °C)

molten zone lengths were approximately 70.0 mm, satisfying the experimental requirements. In contrast, Fig. 7(b) showed that with the main heater and auxiliary heater temperatures set at 700 and 610 °C, respectively, both the simulated and actual molten zone lengths were about 50.0 mm. At this point, the phenomenon of unmelted edges occurred in the molten zone, preventing the purification of that part of the tellurium rod and leading to the migration of impurities to the edge, which is unfavorable.

In addition, it was found that the contact area between the first and last ends of the tellurium rods and the graphite boat was larger, resulting in better heat transfer. As a result, the molten zones formed at both the first and last ends of the tellurium rods were wider under the same conditions. Therefore, during the experiment, the temperature of Heater #1 (the auxiliary heater) should be set lower at the beginning, and the temperature of Heater #3 (also an auxiliary heater) should be appropriately lowered as the experiment progresses toward the end of the tellurium rod. Specifically, when the main heater was at the first end of the tellurium rod (0−100 mm), the temperature of Heater #1 was set as 600 °C. When the main heater reached 100.0 mm from the end of the tellurium rod, the temperature of Heater #3 was reduced to 600 °C.

4.3.1 Main heater (2#) temperature simulation results and experimental analysis

The effect of the main heater temperature on the temperature distribution of the molten zone was investigated, comparing the simulated and actual molten zone lengths, as illustrated in Fig. 8. The auxiliary heater temperature was set as 630 °C, while the main heater temperatures were set as 695, 700, 705, and 710 °C, respectively.

The error between the simulated molten zone length and the actual molten zone length was within 3.0 mm, indicating that the established model was accurate and that the simulation results could effectively guide the experimental process. The experimental results showed that with the auxiliary heater temperature set as 630 °C, when the main heater temperature was less than 695 °C, the molten zone length was under 30.0 mm. However, when the main heater temperature was set to be 700−710 °C, the molten zone length during the refining process could be maintained at 50−60 mm. Therefore, during the experimental process, the temperature of the main heater should be set as 700 °C or higher.

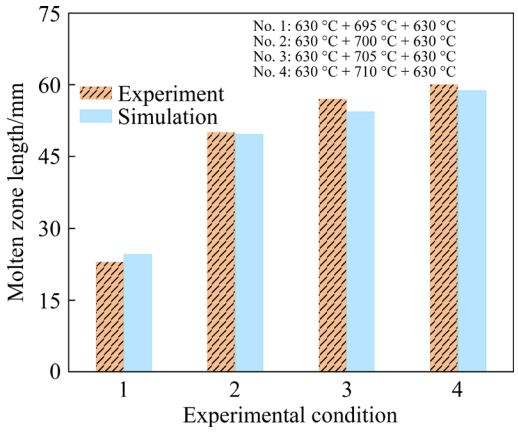

Fig. 8 Comparison of simulated molten zone length and actual molten zone length at different main heater temperatures

4.3.2 Auxiliary heater (1#, 3#) temperature simulation results and experimental analysis

Based on the simulation of the main heater, the effect of the auxiliary heater temperature on the temperature distribution and the length of the molten zone during the tellurium zone refining process was investigated, with the experimental results shown in Fig. 9. The main heater temperatures were set to be 700 and 705 °C, and the auxiliary heater temperatures were set to be 610, 630, and 650 °C, respectively.

As seen from Fig. 9, the simulation results showed a high degree of agreement with the experimental results. When the main heater temperature was set to be 700 °C, the molten zone length was less than 50.0 mm when the auxiliary heater temperature was below 630 °C. However, when the auxiliary heater temperature was between 630 and 650 °C, the molten zone length reached about 60.0 mm, which aligned with the desired molten zone length during the experimental process. When the main heater temperature was 705 °C and the auxiliary heater temperature was between 610 and 630 °C, the molten zone length was about 50 mm. At an auxiliary heater temperature of 650 °C, the molten zone length increased to approximately 80.0 mm, exceeding the theoretical molten zone length for the experimental process. Therefore, when the main heater temperature exceeds 705 °C, the auxiliary heater temperature should be set below 650 °C. Based on this analysis,

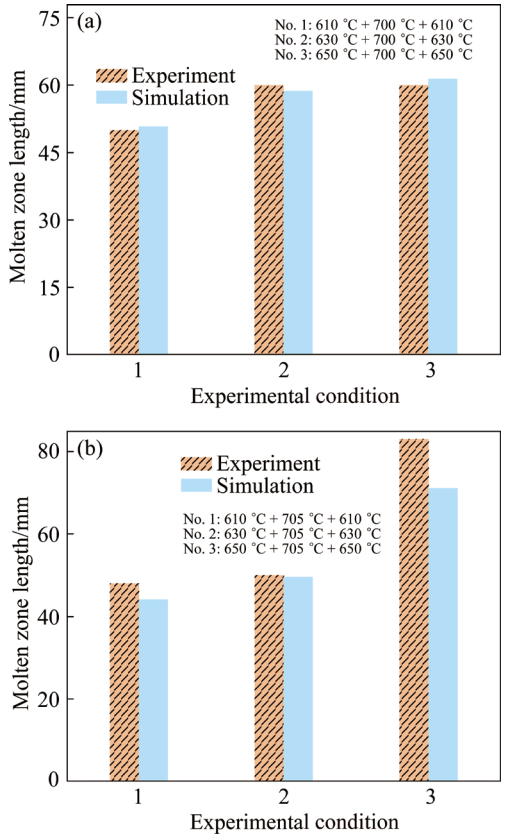

Fig. 9 Comparison of simulated molten zone length and actual molten zone length at different auxiliary heater temperatures

it can be concluded that with the main heater temperature set as 700−710 °C, the auxiliary heater temperature should be maintained at 630−650 °C, which is optimal for controlling the molten zone length during the experiment.

5 Zone refining experiments of tellurium

The molten zone movement speed can affect the shape of the molten zone, and impurity segregation occurs at the solid−liquid interface. The flatter the solid−liquid interface is, the more favorable it is for the migration of impurities to the end of the tellurium rod. The simulation results showed that a stable molten zone can be formed at a main heater temperature of 700−710 °C and an auxiliary heater temperature of 630−650 °C, with a molten zone length of 6−7 cm. Based on this, experimental studies were conducted with molten zone movement speeds of 0.5 and 1.0 mm/min, respectively, and the experimental samples are shown in Fig. 10. The experimental results demonstrate that the distribution of the molten zone during the zone refining process is uniform, thereby further confirming the accuracy of the parameters derived from the simulations.

The purity and total impurity content of tellurium are shown in Fig. 11. After three passes of zone refining, the purity reached 6N, and the impurity removal efficiencies reached 57.8% and 62.3%, respectively. The closer the measurement was to the end of the tellurium rod, the higher the impurity content and the lower the impurity removal efficiency; at the end of the tellurium rod, the removal efficiency was less than 20%. The impurity distribution curve was relatively flat when the molten zone movement rate was 0.5 mm/min; however, when the molten zone movement rate was 1.0 mm/min, the impurity distribution curve was flat at the front end and increased sharply at Position No. 6. It indicates that faster molten zone movement is not favorable for the removal of impurities.

After zone refining, the removal efficiency of impurities is shown in Fig. 12. The removal efficiency of most impurities, such as Ca and Cu, exceeded 95%, while the removal efficiency for impurity P was over 70%, and the removal efficiency for impurity Se was about 50%. From the analysis, it can be observed that after three passes

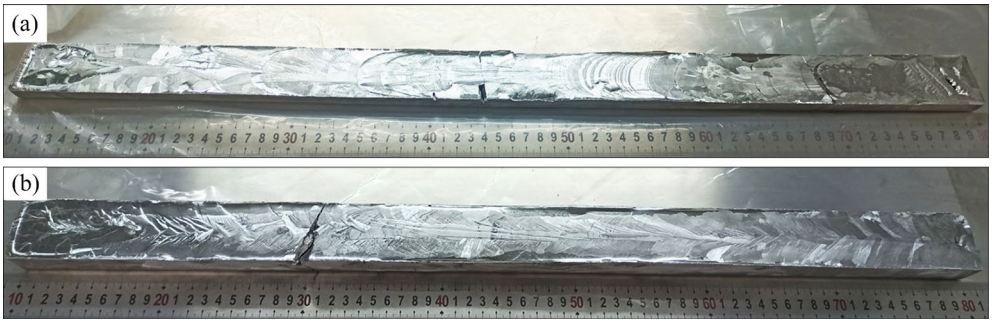

Fig. 10 Photographs of experimental samples at 0.5 mm/min (a) and 1.0 mm/min (b)

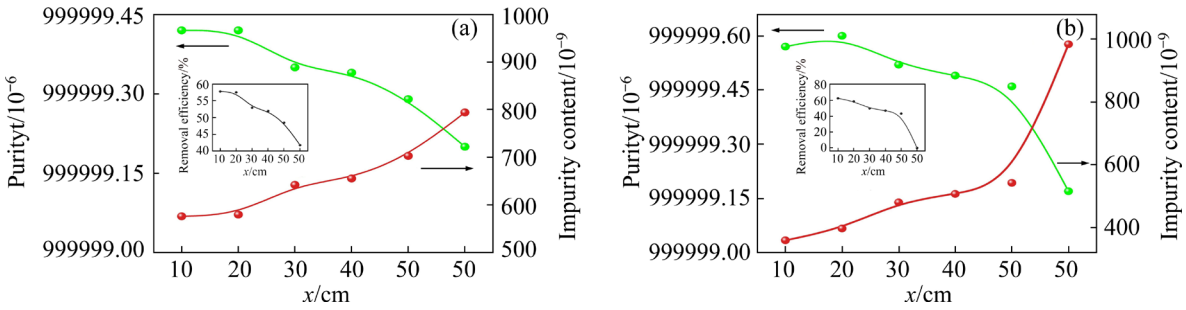

Fig. 11 Purity and total impurity content of tellurium: (a) 0.5 mm/min; (b) 1.0 mm/min

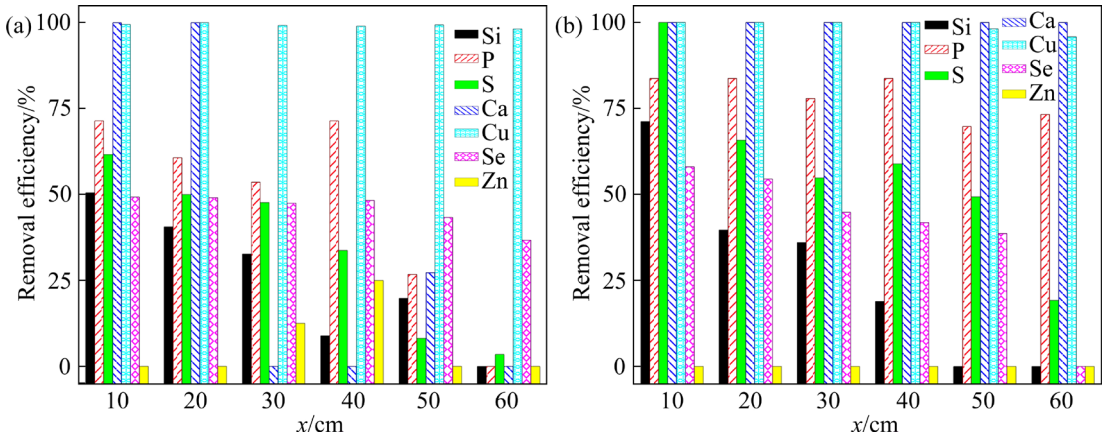

Fig. 12 Removal efficiency of impurities at 0.5 mm/min (a) and 1.0 mm/min (b)

of zone refining, the impurity removal efficiency was similar at molten zone moving speeds of 0.5 and 1.0 mm/min. The number of zone refining passes is too small, resulting in less efficiency in removing impurities. This indicates that the number of zone refining passes had a greater influence on impurity removal efficiency than the molten zone moving speed [30,31].

After zone refining, the impurity content at different locations of the tellurium rods is shown in Table 5. The impurity Se was reduced from 1100 and 846 μg/kg to 558 and 355 μg/kg. The impurity Cu was reduced from 190 and 76 μg/kg to below the instrumental detection limit. The impurity Si was reduced from 10.1 and 11.1 μg/kg to 5.0 and 3.2 μg/kg, respectively, while most of the remaining impurities were reduced to below the instrumental detection limit.

It should be noted that most impurities did not migrate efficiently to the ends of the tellurium rods after three passes of zone refining. Therefore, additional passes of zone refining are needed to effectively enrich the impurities at the ends of the tellurium rods.

Table 5 Contents of impurities at different locations (μg/kg)

Element	0.5 mm/min			1.0 mm/min		
	No.1	No.3	No.5	No.1	No.3	No.5
Li	<0.5	<0.5	<0.5	<0.5	<0.5	<0.5
Na	<0.5	1.50	<0.5	<0.5	<0.5	<0.5
Mg	0.5	<0.5	0.5	<0.5	<0.5	<0.5
Si	5.0	6.8	8.1	3.2	7.1	15.0
P	1.6	2.6	4.1	1.4	1.9	2.6
S	3.3	4.5	7.9	<2	3.3	3.7
Ca	<5	11.0	8.0	<5	<5	<5
Ti	<0.5	1.2	2.2	<0.5	1.0	0.7
Cr	2.1	26.0	43.0	<1	<1	<1
Mn	<0.5	2.7	1.1	<0.5	<0.5	<0.5
Fe	1.0	4.3	1.7	<1	<1	<1
Ni	<0.5	0.9	0.6	<0.5	<0.5	<0.5
Cu	1.0	1.5	1.2	<1	<1	1.4
Zn	3.6	1.2	1.7	<1	<1	<1
Se	558	578	623	355	467	519
Ag	<5	<5	<5	<5	<5	<5
Bi	<5	<5	<5	<5	<5	<5
Total	576.1	642.2	703.1	359.6	480.3	542.4

"<": Below the detection limit of the instrument

6 Conclusions

(1) A simulation model for the zone refining of tellurium was established using COMSOL Multiphysics software. The temperature distribution characteristics of the molten zone were simulated, and validation experiments on the length of the molten zone were conducted. The results showed that a stable molten zone of 6−7 cm was formed under conditions where the temperature of the main heater was 700−710 °C and the temperature of the auxiliary heater was 630−650 °C.

(2) Based on the numerical simulation, zone refining experiments were carried out using 5N tellurium as raw material. The results indicated that the removal efficiency of most impurities, such as Ca and Cu, exceeded 95%. The removal efficiency for impurity P reached over 70%, while the removal efficiency for impurity Se was about 50%. The purity of tellurium reached 6N.

CRediT authorship contribution statement

Qing-hua TIAN: Conceptualization, Methodology, Writing – Review & editing, Funding acquisition; **Zhi-qiang HE:** Conceptualization, Investigation, Methodology, Writing – Original draft, Writing – Review & editing; **Zhi-peng XU:** Conceptualization, Methodology, Writing – Original draft, Writing – Review & editing; **Hai-bei WANG:** Resources and Methodology; **Liu ZHU:** Resources and Methodology.

Declaration of competing interest

The authors declare that they have no known competing financial interests or personal relationships that could have appeared to influence the work reported in this paper.

Acknowledgments

The authors gratefully acknowledge the financial support from the National Key Research and Development Program of China (No. 2023YFC2907904), the National Natural Science Foundation of China (Nos. 52374364, 52104355, 52074363), National Sustainable Development Agenda Innovation Demonstration Zones: Provincial Special “Open Competition” Project in Chenzhou, China (No. 2022sfq57), and Postdoctoral Innovation Talent Support Program, China (No.BX20230438).

References

[1] PEI Jun, CAI Bo-wen, ZHUANG Hua-lu, LI Jing-feng. Bi_2Te_3-based applied thermoelectric materials: Research advances and new challenges [J]. National Science Review, 2020, 7(12): 1856−1858.

[2] SU Meng-yao, LI Xin-yuan, ZHANG Jia-tao. Telluride semiconductor nanocrystals: Progress on their liquid-phase synthesis and applications [J]. Rare Metals, 2022, 41 (8): 2527−2551.

[3] WANG Yong-hua, WANG Gang, ZHOU Yu-feng, XIE Qiao-mu, CHEN Jin-wei, ZHENG Kang-hui, ZHENG Lin, PAN Jin-gong, WANG Rui-lin. Research progress in doped absorber layer of CdTe solar cells[J]. Renewable and Sustainable Energy Reviews, 2023, 183: 113427.

[4] XU Yong-hong, WANG Xin-qing, BI Yan-yu, ZHANG Lin-hui, ZHONG Bin-nian. Simple synthesis and photoelectric properties of Cu_2Te nanotubes [J]. New Journal of Chemistry, 2023, 47: 3010−3016.

[5] HAILS J E, COLE-HAMILTON D J, STEVENSON J, BELL W. Allyl-iso-propyltelluride, a new MOVPE precursor for CdTe, HgTe and (Hg,Cd)Te [J]. Journal of Crystal Growth, 2000, 214/215: 45−49.

[6] SUN Zhao-ming, ZHENG Ya-jie. Preparation of high pure tellurium from raw tellurium containing Cu and Se by chemical method [J]. Transactions of Nonferrous Metals Society of China, 2011, 21(3): 665−672.

[7] ZHANG Xiao-wei, MIAO Rui-ying, WU Dao-gao, ZHU Qiong, WANG Zhi-qiang, CHEN De-hong, YAN Shi-hong. Impurity distribution in distillate of terbium metal during vacuum distillation purification [J]. Transactions of Nonferrous Metals Society of China, 2017, 27(6): 1411−1416.

[8] WAN He-li, KONG Ling-xin, YANG Bin, XU Bao-qiang, DUAN Meng-ping, DAI Yong-nian. Zone melting under vacuum purification method for high-purity aluminum [J]. Journal of Materials Research and Technology, 2022, 17: 802−808.

[9] DUAN Meng-ping, ZHAO Jin-yang, XU Bao-qiang, KONG Ling-xin, YANG Bin, WAN He-li, FU Cheng-cheng. Impurity distribution in the preparation of high-purity aluminum by vacuum zone melting [J]. Transactions of Nonferrous Metals Society of China, 2023, 33: 2843−2852.

[10] WANG Wei-nan, LIU Jun-cheng, SONG Cai-yu. Directionally solidified Al_2O_3/ZrO_2 eutectic ceramic prepared with induction heating zone melting [J]. Journal of Materials Research, 2018, 33(11): 1681−1689.

[11] WANG Yu-bo, JIN Qing-lin, DUAN Xiao-yu, CHEN Yu-chong, LI Zai-jiu, WEN Ming, LIM S. Preparation of high-purity nickel by floating zone refining under a hydrogen atmosphere [J]. Vacuum, 2023, 217: 112557.

[12] TIAN Qing-hua, HE Zhi-qiang, GUO Xue-yi, XU Zhi-peng. Research progress of high purity metals prepared by zone melting [J]. The Chinese Journal of Nonferrous Metals, 2023, 33(10): 3321−3336. (in Chinese)

[13] XU Zhi-peng, JIA Li-li, HE Zhi-qiang, GUO Xue-yi, TIAN Qing-hua. A review of preparing high-purity metals by vacuum distillation [J]. Transactions of Nonferrous Metals Society of China, 2024, 34(5): 1634−1654.

[14] DUAN Meng-ping, ZHAO Jin-yang, XU Bao-qiang, KONG

Ling-xin, YANG Bin, WAN He-li, FU Cheng-cheng. Study on the behavior of impurities in zone melting of aluminum [J]. Journal of Materials Research and Technology, 2022, 21: 3885−3895.
[15] LI Ming-xu, TIAN Qing-le, WU Mei-zhen, PENG Ju-bo, ZHANG Jia-tao, CHEN Li-shi, LU Xing-wei, XU Zhi-shuai, ZHENG Hong-xing. Numerical simulation analysis on solute redistribution of In−1wt.%Sn alloy during multipass vertical zone refining process [J]. Journal of Crystal Growth, 2021, 565: 126156.
[16] LI Ming, LV Guo-qiang, MA Wen-hui, WANG Hua, YANG Xi. Numerical simulation of an unsteady thermal process in vacuum induction furnace for metallurgical grade silicon refining [J]. Applied Mechanics and Materials, 2013, 444/445: 981−985.
[17] CHEN De-hong, YU Chuang, WANG Zhi-qiang, ZHANG Xiao-wei, LU Wen-li, ZHANG Dong-wei. Simulation of lanthanum purification using a finite element method [J]. Materials, 2022, 15(9): 3183.
[18] ROUSSOPOULOS G S, RUBINI P A. A thermal analysis of the horizontal zone refining of indium antimonide[J]. Journal of Crystal Growth, 2004, 271(3/4): 333−340.
[19] GHOSH K, MANI V N, DHAR S. Numerical study and experimental investigation of zone refining in ultra-high purification of gallium and its use in the growth of GaAs epitaxial layers [J]. Journal of Crystal Growth, 2009, 311(6): 1521−1528.
[20] LV Guo-qiang, MA Wen-hui, WANG Hua, MEI Xiang-yang, WEI Kui-xian. Numerical simulation of heat transfer in directional solidification process for polycrystalline silicon [J]. Environmental Engineering and Management Journal, 2011, 10(6): 733−737.
[21] YU Liang, KANG Xiao-an, CHEN Luo-na, LUO Kun, JIANG Yan-li, CAO Xiu-ling. Research status of high-purity metals prepared by zone refining [J]. Materials, 2021, 14(8): 2064.
[22] LIU Y C, DOST S, GRENIER S, AUDET N, HAAS J. A numerical simulation study for the zone refining processes of cadmium and tellurium [J]. International Journal of Materials and Product Technology, 2008, 32(1): 1−19.
[23] EZHEIYAN M, SADEGHI H, TAVAKOLI M H. Thermal analysis simulation of germanium zone refining process assuming a constant radio-frequency heating source [J]. Chinese Physics Letters, 2016, 33(5): 058102.
[24] TIAN Qing-hua, HE Zhi-qiang, XU Zhi-peng, LI Dong, GUO Xue-yi. Experimental analysis of high purity tellurium prepared by zone refining [J]. Metallurgical and Materials Transactions B, 2024, 55: 772−781.
[25] PRASAD D S, MUNIRATHNAM N R, RAO J V, PRAKASH T L. Effect of multi-pass, zone length and translation rate on impurity segregation during zone refining of tellurium [J]. Materials Letters, 2006, 60(15): 1875−1879.
[26] ZHANG Huan, ZHAO Jin-yang, XU Jun-jie, LI Yi-fu, PU Zheng-hao, XU Bao-qiang, YANG Bin. Preparation of high-purity tin by zone melting [J]. Russian Journal of Non-Ferrous Metals, 2020, 61(1): 9−20.
[27] WANG Shun-heng, CHU Zong-fu, LIU Jun-cheng. Microstructure and mechanical properties of directionally solidified Al_2O_3/$GdAlO_3$ eutectic ceramic prepared with horizontal high-frequency zone melting [J]. Ceramics International, 2019, 45(8): 10279−10285.
[28] ZHANG Xiao-xin, FRIEDRICH S, FRIEDRICH B. The influence of initial purity level on the refining efficiency of aluminum via zone refining [J]. Metals, 2021, 11(2): 201.
[29] CHOI H G, SHIM M, LEE J H, YI K W. Numerical analysis of impurity separation from waste salt by investigating the change of concentration at the interface during zone refining process [J]. Journal of Crystal Growth, 2017, 474: 69−75.
[30] GHOSH K, MANI V N, DHAR S. A computational study and experimental validation of zone refining process for ultra-purification of gallium for opto-electronic applications [J]. Transactions of the Indian Institute of Metals, 2008, 61: 201−206.
[31] GHOSH K, MANI V N, DHAR S. A modeling approach for the purification of group III metals (Ga and In) by zone refining [J]. Journal of Applied Physics, 2008, 104(2): 024904.

基于模拟辅助区域熔炼制备高纯碲

田庆华[1]，何志强[1]，许志鹏[1]，王海北[2]，朱 刘[3]

1. 中南大学 冶金与环境学院，长沙 410083；
2. 矿冶科技集团有限公司，北京 100160；
3. 广东先导稀材股份有限公司，清远 511517

摘 要：通过模拟研究温度对熔区长度的影响，优化实验过程对熔区长度的控制。采用 COMSOL Multiphysics 软件模拟了区域熔炼过程中熔区的温度梯度分布特征，并进行了实验验证。模拟的熔区长度与实际的熔区长度吻合良好。在区域熔炼次数为 3 次、氢气流量为 0.5 L/min、熔区移动速度分别为 0.5 和 1.0 mm/min 的条件下，开展了区域熔炼提纯碲的实验研究。结果表明，Ca 和 Cu 等杂质的脱除率可达 95%以上，杂质 P 的脱除率可达 70%以上，碲的纯度达到 6N。

关键词：高纯碲；模拟；区域熔炼；熔区长度

(Edited by Xiang-qun LI)